

## Galactic cosmic-ray flux short-term variations and associated interplanetary structures with LISA Pathfinder

C. GRIMANI<sup>(1)(2)</sup>, S. BENELLA<sup>(1)(2)</sup>, M. FABI<sup>(1)</sup>, N. FINETTI<sup>(2)(3)</sup>,  
M. LAURENZA<sup>(2)(4)</sup>, D. TELLONI<sup>(2)(5)</sup> and M. VILLANI<sup>(1)(2)</sup>

<sup>(1)</sup> *Università degli Studi di Urbino “Carlo Bo” - Urbino, Italy*

<sup>(2)</sup> *INFN, Sezione di Firenze - Sesto Fiorentino, Italy*

<sup>(3)</sup> *Università degli Studi dell’Aquila - L’Aquila, Italy*

<sup>(4)</sup> *Istituto di Astrofisica e Planetologia Spaziali, INAF - Roma, Italy*

<sup>(5)</sup> *Osservatorio Astronomico di Torino, INAF - Torino, Italy*

received 28 December 2018

**Summary.** — The European Space Agency LISA Pathfinder (LPF) mission orbited around the Sun-Earth first Lagrangian point L1 between January 2016 and July 2017. A particle detector aboard LPF allowed for galactic cosmic-ray (GCR) integral flux measurements above 70 MeV n<sup>-1</sup> between 2016 February 18 and 2017 July 3 during the descending phase of the present solar cycle N. 24, which is characterized by a positive polarity period. The statistical uncertainty on hourly-averaged GCR countings was of 1%. The characteristics of recurrent and non-recurrent GCR flux short-term variations observed with LPF are reported here. In particular, it is focused on GCR flux variation profiles and their association with the passage of large-scale interplanetary structures. Forbush decrease observations and geomagnetic storm occurrence during LPF are also briefly discussed.

### 1. – Introduction

LISA Pathfinder (LPF) [1, 2] was the technology mission of the European Space Agency (ESA) for testing the performance of instruments that will be placed aboard LISA, the Laser Interferometer Space Antenna for gravitational wave detection in space [3]. LPF was launched from the Kourou base in French Guiana on 2015 December 3 and reached its final orbit around the Lagrange point L1, at 1.5 million km from Earth in the Earth-Sun direction, after approximately two months. The LPF elliptical orbit, with major and minor axes of  $8 \times 10^5$  km and  $5 \times 10^5$  km, respectively, was inclined by about 45 degrees to the ecliptic plane. The mission ended on 2017 July 18. LPF carried two 2-kg cubic gold-platinum free-floating test masses (TMs) that played the role of mirrors of the interferometer. The aim of the LPF mission was to measure spurious

forces limiting the sensitivity of the interferometer for LISA. Coulombian forces due to the TM charging induced by the interactions of energetic particles of solar and galactic origin were expected to be one of the main sources of noise for the experiment during solar energetic particle events. The TMs were surrounded by  $13 \text{ g cm}^{-2}$  of matter that limited the minimum energy of protons and ions (constituting 98% in composition of the bulk of both solar and galactic particle samples) reaching and charging the test-masses to  $100 \text{ MeV n}^{-1}$ . In order to monitor *in situ* the overall particle incident flux on the spacecraft, a particle detector (PD) was mounted behind the solar panels aboard LPF. The PD consisted of two silicon wafers with dimensions  $1.4 \times 1.05 \times 0.03 \text{ cm}^3$ , located inside a shielding copper box of 6.4 mm thickness that stopped particles with energies smaller than  $70 \text{ MeV n}^{-1}$  [4]. This conservative choice was made in order not to underestimate the actual particle flux reaching and charging the test-masses. The PD allowed for the counting of protons and helium nuclei traversing each silicon layer (single counts) and for the measurement of ionization energy losses of particles passing through both silicon wafers (coincidence mode). The single counts were gathered with a sampling time of 15 s and ionization energy losses of events in coincidence mode were stored in the form of histograms on the on-board computer and then returned to the telemetry every 600 s. The maximum allowed detector counting rate was  $6500 \text{ counts s}^{-1}$  on both silicon wafers corresponding to an event integrated proton fluence of  $10^8 \text{ protons cm}^{-2}$  at energies  $> 100 \text{ MeV}$ . In coincidence mode 5000 energy deposits was the saturation limit. For particle energies  $> 100 \text{ MeV n}^{-1}$  the PD geometrical factor was found to be energy independent and equal to  $9 \text{ cm}^2 \text{ sr}$  for an isotropic particle incident flux on each silicon wafer. In coincidence mode the detector geometrical factor was about one tenth of this value. PD data were gathered between 2016 February 18 and 2017 July 3.

This paper is organized as it follows: in sect. 2 the galactic cosmic-ray (GCR) energy spectra estimated before the LPF launch for the period 2016-2017 and their comparison with observations are presented; in sect. 3 it is focused on GCR short-term recurrent and non-recurrent variations observed with LPF and, finally, in sect. 4 is reported the geomagnetic storm and Forbush decrease occurrence when LPF was in orbit.

## 2. – GCR energy spectra during LPF

GCR flux observations in the inner heliosphere present long-term ( $> 1$  year) and short-term ( $< 1$  month) variations. Long-term variations are associated with the 11-year solar cycle and with the 22-year solar polarity reversal [5]. During positive polarity periods, the symmetric model in the *force field approximation* by Gleeson and Axford (G&A) [6] was found to reliably reproduce the trend of the proton and helium energy differential fluxes observed with a series of balloon flights of the BESS and BESS-Polar experiments [7]. This model shows that at 1 AU the effect of the solar modulation on single charged particle fluxes in rigidity (particle momentum per unit charge) above 100 MV is completely defined by a solar modulation parameter  $\phi$  that, at these energies, is associated with the particle energy loss parameter from the interstellar medium to the point of observation. By assuming the same solar modulation parameter for proton and helium energy spectra, the G&A model was applied for LPF to the time-independent interstellar intensities estimated in [7] at the beginning (2015 December-2016 January;  $\phi = 550 \text{ MV}$ ) and at the end (2017 July;  $\phi = 320 \text{ MV}$ ) of the mission [8]. The proton and helium energy spectra thus obtained are shown in fig. 1 after interpolation with the

function reported in eq. (1):

$$(1) \quad F(E) = A(E + b)^{-\alpha} E^{\beta} \quad \text{particles (m}^2 \text{ sr s GeV n}^{-1}\text{)}^{-1}.$$

The above cosmic-ray energy spectra parameterization is well representative of the GCR observations trend in the inner heliosphere between a few tens of MeV and hundreds of GeV within experimental errors [9]. The  $A$ ,  $b$ ,  $\alpha$  and  $\beta$  model parameters at the time of LPF are listed in Table I. Predictions for 2015 December - 2016 January were compared to observations carried out with an independent analysis of the LPF data [10] after the end of the mission and preliminary AMS data for January 2016 presented at COSPAR 2018 (2018 July 14-22, Pasadena). A very good agreement between observations and predictions is observed.

TABLE I. – *Parameterization of proton and helium energy spectra predictions at the beginning and at the end of the LPF mission [11].*

	$A$	$b$	$\alpha$	$\beta$
p (2015 December-2016 January)	18000	1.19	3.66	0.87
p (2017 July)	18000	0.82	3.66	0.87
He (2015 December-2016 January)	850	0.96	3.23	0.48
He (2017 July)	850	0.68	3.23	0.48

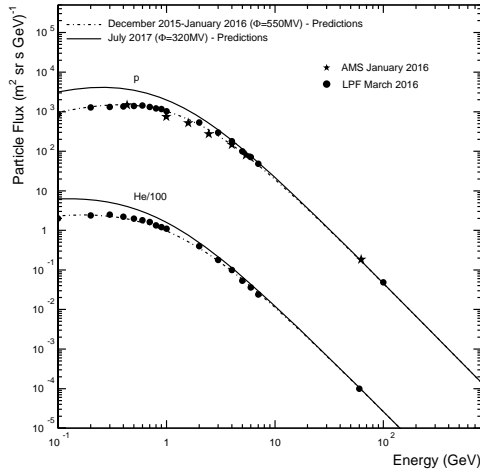


Fig. 1. – GCR proton and helium energy spectra estimated before mission launch [8] for the beginning (2015 December-2016 January; dot-dashed lines) and the end of the LPF mission (2017 July; continuous lines). The helium flux appears properly scaled in order not to superpose lines. Predictions are compared to observations: solid dots correspond to March 2016 LPF data estimated after mission end [10] and solid stars are the AMS experiment preliminary data for January 2016 (presented at COSPAR 2018, Pasadena).

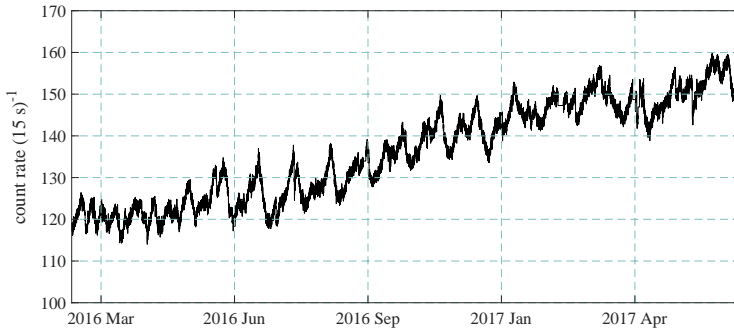


Fig. 2. – Hourly averaged GCR 15 s count rate observed with the LPF PD.

### 3. – GCR short-term variations aboard LPF

The whole GCR data sample gathered with LPF at a frequency of 0.067 Hz is shown in fig. 2.

**3.1. Recurrent variations.** – Recurrent GCR variations were studied by using the empirical mode decomposition (EMD) technique [12]. This technique is based on the assumption that any time series can be represented by a superposition of monocomponent signals  $C_i(t)$ , called intrinsic mode functions, characterized by a well-defined mean period of oscillation  $\tilde{\tau}_i$ . When all the intrinsic mode functions in the original data set are subtracted, the remaining function is called residue of the decomposition  $res(t)$ . The residue does not complete any oscillation in the selected time domain and consists of a monotonic function or a function with only one maximum and one minimum representing the trend of the data. By applying the EMD technique to white noise or fractional Gaussian noise, the product between the energy density of each intrinsic mode function,  $E_i = \langle |C_i(t)|^2 \rangle_t$ , and its corresponding mean period  $\tilde{\tau}_i$  is constant [13, 14]. In Table II are reported the mean oscillation periods present in the LPF GCR data: intrinsic mode functions # 7-9 show that periodicities of 9, 13.5, and 27 days (within errors), related to the Sun rotation and higher harmonics periodicities, are present. The application of the Wu and Huang [13] method allows to quantify the statistical significance of modes

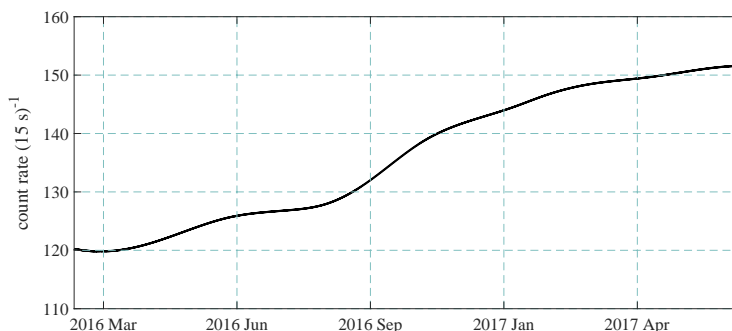


Fig. 3. – Residue of the EMD analysis of the GCR data from LPF.

TABLE II. – Mean oscillation periods of the intrinsic mode functions in the EMD of the GCR LPF data with the standard error.

mode # $i$	mean period $\tilde{\tau}_i$ (days)	mode # $i$	mean period $\tilde{\tau}_i$ (days)
1	$0.12 \pm 0.01$	7	$10.3 \pm 0.3$
2	$0.21 \pm 0.01$	8	$14.1 \pm 0.6$
3	$0.41 \pm 0.01$	9	$27.6 \pm 1.0$
4	$0.81 \pm 0.01$	10	$46.3 \pm 3.0$
5	$1.76 \pm 0.03$	11	$87.9 \pm 7.1$
6	$3.8 \pm 0.1$		

with respect to white noise. The intrinsic mode functions 6-11 lie above the 99% white noise spread line. Fig. 3 shows the residue obtained with the EMD technique: the GCR count rate presents an increasing trend over the mission lifetime due to the decreasing solar activity. The average duration of the recurrent GCR flux short-term variations was found to be  $9.2 \pm 5.0$  days and the average intensity was of  $5.1 \pm 2.5$  %. As it can be observed in fig. 4, the main role in generating short-term recurrent GCR flux variations was played by corotating interaction regions and high-speed solar wind streams (HSS) passage [11].

**3.2. Non-recurrent variations.** – Non-recurrent sudden drops of the GCR intensity due to the passage of interplanetary coronal mass ejections (ICMEs) and interplanetary shocks are called Forbush decreases (FDs) [15]. Three FDs were observed with LPF on 2016 July 20, 2016 August 2 and 2017 May 27 (see Fig. 4). Details and characteristics of the 2016 August 2 FD are reported in [11, 16]. Twenty-three non-recurrent short-term variations (6 peaks and 17 hollows) shorter than two days were also observed (see for

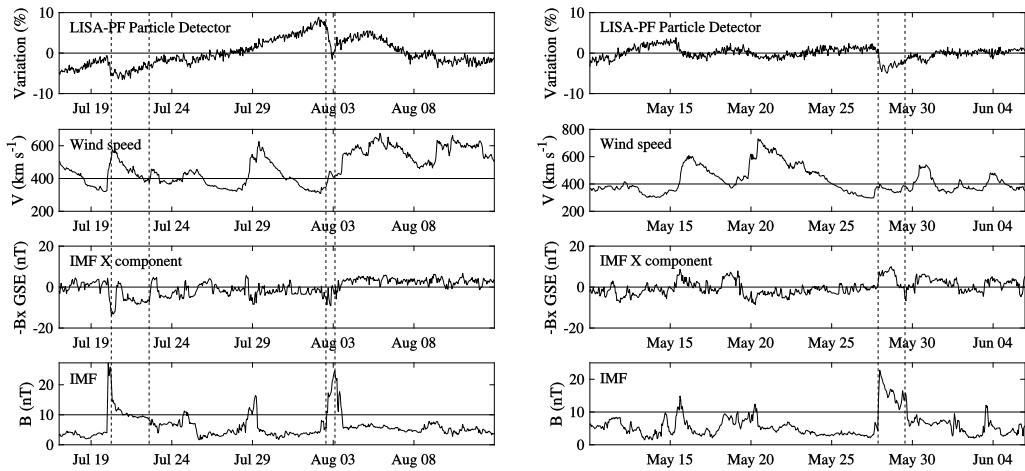


Fig. 4. – LPF GCR flux fractional variations (top panels) during the Bartels rotations 2496 (left) and 2507 (right). The vertical dashed lines indicate the passage of three near-Earth ICMEs (<http://www.srl.caltech.edu/ACE/ASC/DATA/level3/icmetable2.htm>) with associated FDs. In the other panels are reported the solar wind speed, magnetic field x component and intensity observed with the ACE satellite.

instance a small peak on 2016 August 8 on the left panel of fig. 4). Hollows appear to be associated with heliospheric current sheet crossing in the majority of cases while peaks were correlated with compressed plasma regions between HSS.

#### 4. – FDs and geomagnetic storm occurrence during LPF

Two medium-strong geomagnetic storms occurred during LPF: on 2016 October 13 (Dst=-102 nT) and 2017 May 27 (Dst=-122 nT). A FD was observed aboard LPF in the second case only (right panel in fig. 4). In general FDs could be used to forecast geomagnetic storms when the increase of the interplanetary magnetic field (IMF) intensity, responsible for the GCR flux depression, is associated with a large, negative z-component of the IMF reconnecting with the Earth magnetic field.

#### 5. – Conclusions

A PD aboard the ESA LPF mission allowed for the study of GCR flux recurrent and non-recurrent short-term variations in the L1 Lagrange point between 2016 February 18 and 2017 July 3 during the descending part of the solar cycle N. 24. Recurrent variations were associated with HSS transit while three FDs were correlated with the passage of near-Earth ICMEs.

\* \* \*

The LPF data can be downloaded from  
<https://www.cosmos.esa.int/web/lisa-pathfinder-archive/home>.  
 Sunspot number and solar modulation parameter data were gathered from  
<http://www.sidc.be/silso/home>  
 and [http://cosmicrays.oulu.fi/phi/Phi\\_mon.txt](http://cosmicrays.oulu.fi/phi/Phi_mon.txt), respectively.  
 HCS crossing was taken from  
[http://omniweb.sci.gsfc.nasa.gov/html/polarity/polarity\\_tab.html](http://omniweb.sci.gsfc.nasa.gov/html/polarity/polarity_tab.html).  
 Data from the ACE experiment were obtained from the NASA-CDAWeb website.

#### REFERENCES

- [1] ARMANO, M. *et al.*, *Physical Review Letters*, **116** (2016) 23: 231101;
- [2] ARMANO, M. *et al.*, *Physical Review Letters*, **120** (2018) 6: 061101;
- [3] AMARO-SEOANE, P. *et al.*, *arXiv:1702.00786*, (2017) ;
- [4] CANIZARES, P. *et al.*, *Classical Quantum Gravity*, **28** (2011) 9: 094004;
- [5] GRIMANI, C. , *Astronomy & Astrophysics*, **474** (2007) : 339-343;
- [6] GLEESON, L.J., AXFORD, W.I., *Journal of Geophysical Research*, **81** (1976) 19: 3403-3406;
- [7] SHIKAZE, Y. *et al.*, *Astroparticle Physics*, **28** (2007) 1: 154-167;
- [8] GRIMANI, C. *et al.*, *Classical Quantum Gravity*, **32** (2015) : 035001 (11pp);
- [9] PAPINI P., GRIMANI C., and STEPHENS S.A., *Il Nuovo Cimento C*, **19** (1996) 3: 367-387;
- [10] ARMANO, M. *et al.*, *Astroparticle physics*, **98** (2018) 28-37;
- [11] ARMANO, M. *et al.*, *Astrophysical Journal*, **854** (2018) 2: 113 (12pp);
- [12] HUANG, N.E. *et al.*, *Proceedings of the Royal Society of London A: mathematical, physical and engineering sciences*, **454** (1998) 1971: 903-995.
- [13] WU, Z., HUANG, N.E., *Proceedings of the Royal Society of London A: mathematical, physical and engineering sciences*, **460** (2004) 2046: 1597-1611.
- [14] FLANDRIN, P. *et al.*, *IEEE signal processing letters*, **11** (2004) 2: 112-114.
- [15] CANE H.V., in *Cosmic Rays and Earth* (Springer) 2000, pp. 55-77.
- [16] BENELLA, S. *et al.*, these proceedings.